Oct 26th

Post-Buckling in the Distortional Mode and Buckling Mode Interaction of Cold-Formed Thin-Walled Sections with Edge Stiffeners

Derrick C. Y. Yap

Gregory J. Hancock

Eighteenth International Specialty Conference on Cold-Formed Steel Structures
Orlando, Florida, U.S.A, October 26 & 27, 2006

Post-Buckling in the Distortional Mode and Buckling Mode Interaction of Cold-Formed Thin-Walled Sections with Edge Stiffeners

Derrick C.Y. Yap[1] and Greg J. Hancock[2]

Abstract

The buckling modes of cold-formed thin-walled sections with edge stiffeners generally occur at distinct lengths, but interaction of buckling modes may be present at certain lengths. This may be due to the distortional mode interacting with the local buckling mode, both of which may be in the post-buckling range. The paper discusses the analysis of post-buckling in the distortional mode of a thin-walled section with edge stiffeners and the effect of interaction of buckling modes on failure loads. The analysis is based on the longitudinal stress development and redistribution using the finite element package ABAQUS. This methodology whereby the longitudinal stress redistribution is studied is similar to the work of Von Karman et al, in predicting the post-local buckling behaviour.

Introduction

Thin-walled sections such as lipped channels can buckle in three different modes being the short half-wavelength local buckle, the intermediate half-wavelength distortional buckle and the long half-wavelength flexural/flexural-torsional buckle (Hancock, Murray and Ellifritt (2001), Hancock (2003), Schafer (2002)). The local buckling mode has been well researched and an effective width model developed by Von Karman et al (1932) to produce a simple model

[1] PhD student, School of Civil Engineering, University of Sydney, NSW, Australia
[2] BlueScope Steel Professor of Steel Structures, School of Civil Engineering, University of Sydney, NSW, Australia

of the post-buckling reserve strength. The flexural-torsional mode has been well researched by Timoshenko (1945), Vlasov (1961) and Trahair (1993) and was shown to have very little postbuckling reserve of strength. The distortional buckling mode has been researched at the University of Sydney in recent years by Hancock (1985), Lau and Hancock (1990), Kwon and Hancock (1992) and Yang and Hancock (2004), at Johns Hopkins University by Schafer (2002) and the Technical University of Lisbon, Portugal by Camotim and Silvestre (2004). What has been known for some time is that the distortional mode has a postbuckling strength which is generally less than that of local buckling. However, the nature of this postbuckling reserve is not clearly understood, particularly what precipitates failure.

Sridharan (1982) demonstrated that soon after buckling in the distortional mode, yielding occurs in the lip either at the tip or the flange junction depending on which way the flange and lip move (inward or outward respectively). He concluded that "one likely consequence of buckling of an edge stiffener in its own plane would be the onset of plastic yielding; and the yielding of a member which has been the main source of stiffness cannot but hasten the collapse of the structure". However, experimentation such as that of Yang and Hancock (2004) has shown experimentally this not to be the case with substantial postbuckling reserve in line with the early work of Kwon and Hancock (1992) even when the lip has yielded and developed local plastic mechanisms. A further complication raised by Yang and Hancock was the difference between the strength when the lips moved inward generally with a lower strength than when they moved outward. This was confirmed theoretically more recently by the Generalised Beam Theory (GBT) models of Silvestre and Camotim (2004) for fixed ended sections.

The main purpose of this paper is to investigate postbuckling in the distortional mode using the finite element program ABAQUS. The distortional mode cannot be completely isolated from the local mode and so the interaction of local and distortional buckling is considered in the paper. The work of Von Karman et al. (1932) showed that the postbuckling behaviour could be explained by looking at the longitudinal stress redistribution around the section in the postbuckling range of behaviour. The same approach is used in this paper. In addition, strength design curves for distortional buckling of channels in compression are further validated against the ABAQUS models.

Sections investigated

The basic section chosen was a simple lipped channel with an 80 mm web and 60 mm flange. It was decided to study 6 mm, 3 mm and 2 mm thick sections

with 9 mm lip, and 2 mm and 1 mm thick sections with 5 mm lip. These dimensions were chosen to produce pure distortional buckling in some cases (i.e. 6 mm thick section) and interaction buckling in some cases (i.e. 2 mm with 9 mm lip, 1 mm with 5 mm lip). Fig. 1 shows the buckling stress versus buckled half-wavelength for the 1 mm thick section with 5 mm lip. The section was analysed using the semi-analytical finite strip method (SAFSM), shown as the solid line, and the spline finite strip (SFSM), shown as a line with circles. It can be seen that with the fixed ended condition of the SFSM, the distortional buckling stress increased and is similar to the local buckling stress. This would allow for possible interaction of local and distortional buckling modes. All sections were analysed with one buckle half-wave at 300 mm, except for the 3 mm thick section, which was analysed at 400 mm.

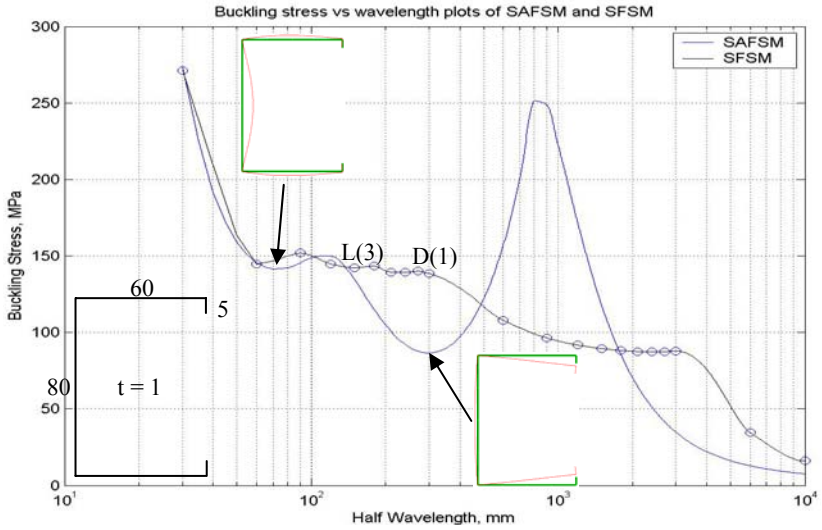

Figure 1 Plot of buckling stress vs half-wavelength for 1 mm thick section with 5 mm lip

Finite element analysis

The finite element model set up has been discussed by Yap and Hancock (2006). The paper noted that plastic strains were included for the inelastic analysis and the plastic strain data was based on Yang and Hancock (2006) stress-strain curves of G550 coupons in tension. The yield stress is assumed to be 700 MPa.

The model uses S4R shell elements. The web and flanges have a mesh size of approximately 5 mm x 5 mm and the lips have mesh sizes ranging from 5 mm x

2.5 mm to 5 mm x 4.5 mm. The column was assumed to be compressed between fixed ends, with all nodes at the ends fixed except the translational degree of freedom at the top of the column. A geometric imperfection magnitude of 0.15t was applied to the model.

Sensitivity and validation analyses

Geometric imperfections are included in the finite element model by linear superposition of buckling modes. A scaling factor with respect to the thickness was applied to the imperfection before superimposing to create the perturbed mesh. To validate the analyses and investigate imperfection magnitudes, sensitivity and validation analyses were preformed with different levels of geometric imperfections.

As part of this investigation, both outwards (O-O) and inwards (I-I) imperfections have been assumed where outwards refers to the lip motion relative to the other lip. Schafer and Pekoz (1998) recommended that for a distortional geometric imperfection (called Type 2), a value approximately equal to the plate thickness, *t*, can be chosen. However this value may be too large when applied as the maximum amplitude of a distortional buckling half-wave since it may produce conservative results for distortional buckling modes with increasing material thickness. A value of *0.64t* was obtained by Schafer and Pekoz from the lower bound probability of 25 % of the Type 2 imperfections and this value has been used to analyse and compare the FEA ultimate failure loads to known strength curves in Fig. 2. The curves are a strength curve (P_{uw}) based on the Winter (1968) effective width formula and the Kwon and Hancock (1992) strength equation (P_{ukh}) , which is the same as used in the Direct Strength Method (DSM) in AS/NZS 4600:2005 (2005) and NAS (supplement) (2004). The elastic buckling curve (P_{od} or P_{ol}) is shown as the solid line, while the Winter strength curve, for local buckling, is shown as the line with triangles (▲) and the Kwon and Hancock strength curve, for distortional buckling, as a line with circles (●). The Winter strength curve is derived from the Winter (1968) effective width as shown in Equations 1 and 2.

$$\frac{b_e}{b} = 1 \qquad \lambda_l \le 0.673 \qquad (1)$$

$$\frac{b_e}{b} = \sqrt{\frac{f_{ol}}{f_y}}\left(1 - 0.22\sqrt{\frac{f_{ol}}{f_y}}\right) \qquad \lambda_l > 0.673 \qquad (2)$$

where, $\lambda_l = \sqrt{\frac{f_y}{f_{ol}}}$, f_y is the yield stress and f_{ol} is the local buckling stress

When the effective width, b_e, of each element of a section is computed for each element in the section assuming that all buckle locally at the same stress f_{ol}, then multiplying by the plate thickness, t, and yield stress, f_y, and summing over all elements in the section produces

$$P_{uw} = P_y \qquad \lambda_l \le 0.673 \qquad (3)$$

$$P_{uw} = \sqrt{\frac{P_{ol}}{P_y}}\left(1 - 0.22\sqrt{\frac{P_{ol}}{P_y}}\right)P_y \qquad \lambda_l > 0.673 \qquad (4)$$

where,

$$\lambda_l = \sqrt{\frac{P_y}{P_{ol}}}, \quad P_y = Af_y \text{ and } P_{ol} = Af_{ol}$$

Equations 3 and 4 are called the Winter strength equations in this paper and apply to local bucking.

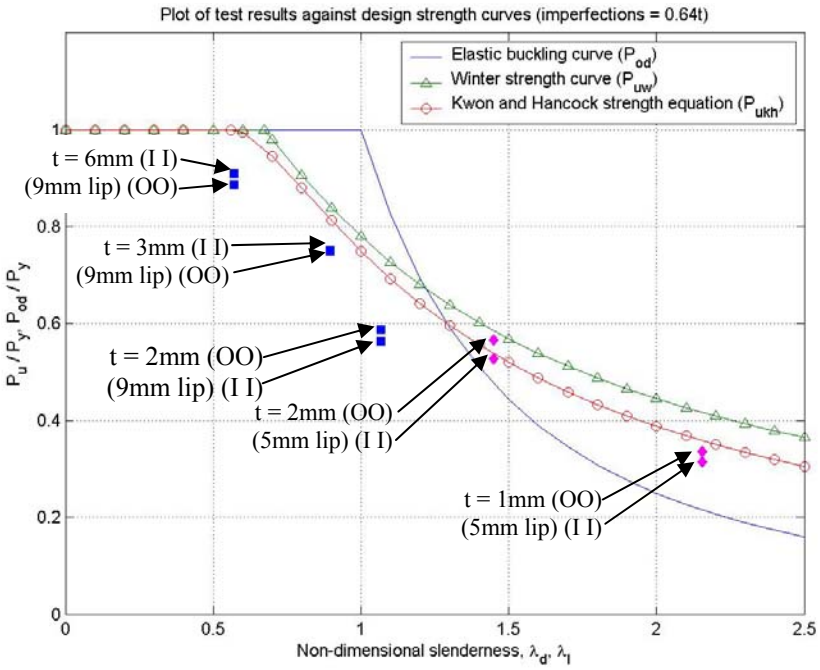

Figure 2 FEA results compared to strength curves with imperfection 0.64t

Equations 5 and 6 are the Kwon and Hancock strength equations and are similar to Equations 3 and 4 except that the coefficient 0.22 and the exponent 0.5 have been changed to 0.25 and 0.22 respectively lower the curve below the Winter strength equations and P_{ol} has been replaced by the distortional buckling load $P_{od} = Af_{od}$.

$$P_{ukh} = P_y \qquad \lambda_d \le 0.561 \qquad (5)$$

$$P_{ukh} = \left[1 - 0.25\left(\frac{P_{od}}{P_y}\right)^{0.6}\right]\left(\frac{P_{od}}{P_y}\right)^{0.6} P_y \qquad \lambda_d > 0.561 \qquad (6)$$

where,

$\lambda_d = \sqrt{\frac{P_y}{P_{od}}}$, $P_{od} = Af_{od}$ and f_{od} is the distortional buckling stress

Silvestre and Camotim (2004) also investigated the local and distortional postbuckling behaviour of lipped channel columns using Generalised Beam Theory (GBT) and finite element analyses. In their paper, the geometric imperfections were assumed to have an amplitude of 0.15t which was applied to the finite element models for both the local and distortional buckling mode analyses. The FEA ultimate failure loads based on an imperfection of 0.15t are compared with the strength curves in Fig. 3 and are higher than those in Fig. 2 based on the 0.64t.

It can be seen in Figs. 2 and 3 that at higher slenderness, the FEA results for columns with both imperfection magnitudes are slightly lower than the Kwon and Hancock strength curve. When the columns with 9 mm lips are analysed at a thickness of 2 mm, it can be seen from Figs. 2 and 3 that the ultimate loads are significantly lower compared to the Kwon and Hancock strength curve for both imperfection magnitudes. With thickness increasing to 3 mm and 6 mm, it can be seen from Fig. 2 that the analyses with an imperfection magnitude of 0.64t produced much lower ultimate loads when compared to the strength curves, whereas analyses with an imperfection magnitude of 0.15t produced ultimate loads that are well predicted by the strength curves as seen in Fig. 3. Some of these differences are due to the imperfection magnitudes but some are due to interaction buckling and will be discussed in more detail later in this paper.

The sensitivity analysis confirms the initial statement that thinner materials (1 mm or less) is less sensitive to imperfection magnitudes as the difference in ultimate loads are relatively similar. However with thicker materials, the ultimate loads are sensitive to imperfections and with a larger imperfection, the FEA ultimate loads becomes lower when compared to the strength curves.

Generally the scale factor of 15 % of the plate thickness provides ultimate loads which compare well with the strength curves which are based on tests. Therefore, the scale factor of 15 % of the plate thickness is chosen as the maximum amplitude of the geometric imperfections in the distortional mode to be applied to the finite element models for the later analyses in this paper. This choice is particularly important in this paper because thicker sections have been chosen in many of the analyses to separate the local and distortional modes.

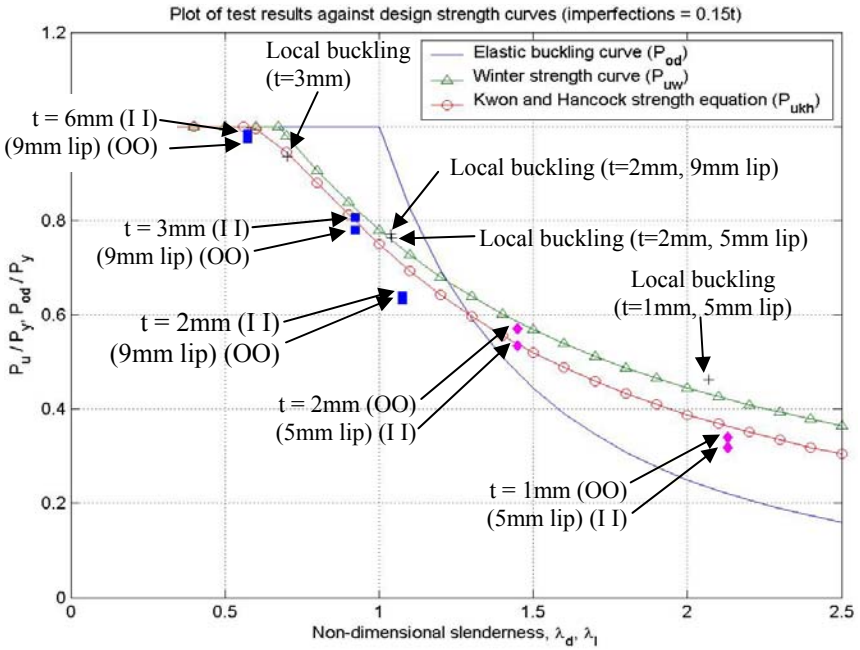

Figure 3 FEA results compared to strength curves with imperfections 0.15t

To compare the FEA analyses with the Winter strength curve for local buckling, a set of additional analyses where distortional buckling was prevented was performed. From Fig. 3, it can be seen that the local buckling strength, shown as a plus (+) symbol, for the sections with varying thicknesses are well predicted by the Winter strength curve based on a slenderness λ_l for local buckling of the whole section. For sections with thicknesses 1 mm and 2 mm, the FEA ultimate loads are slightly higher, whereas for the section at 3 mm thickness, the FEA ultimate load is slightly lower, which is most likely due to assumed imperfections.

Load deflection curves

The load-deflection curves for the postbuckling analyses for the 3 mm and 1 mm thick sections are shown in Figs. 4 and 5 respectively. In each figure, the inward and outward curves are plotted for a material that is assumed to remain elastic and with yielding also included. The inward and outward deflecting curves for the elastic material are defined as the square ( ) and diamond ( ) lines respectively. Similarly the inward and outward deflecting curves for the material with yielding included are defined as the star ( ) and cross ( ) lines respectively.

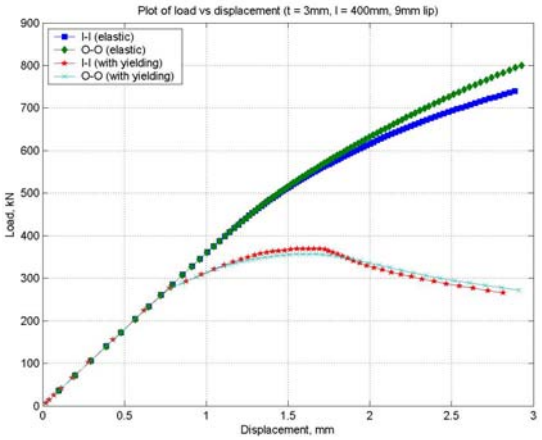

Figure 4 Load deflection curves for section with t = 3mm

Comparing Figs. 4 and 5, it can be noted that as the sections get thinner, the elastic postbuckling curves become more separated with the inward curve always below the outward curve. This is due to the different stress redistributions across the section for the inward and outward deflection cases and will be further discussed. For the material with yielding included, the sections with thickness 6 mm, 3 mm and 2 mm with 9 mm lip failed below the critical distortional stress while sections with thickness 2 mm with 5 mm lip and 1 mm with 5 mm lip failed in the post-distortional stress range. For the 3 mm thick section, it can be noted in Fig. 4 that the inward curve is higher than the outward curve at failure, but very quickly the curves cross over with the outward curve carrying more load after failure. It is interesting to note that this cross over point approaches the elastic curves as the material gets thinner. For the 1 mm thick section, this cross over occurs in the elastic curve, hence it can be seen

in Fig. 5 that the outward curve is higher than the inward curve at failure. This shows that in the post-distortional buckling mode, the outward deflecting sections are stiffer than the inward deflecting sections. This confirms the results from Yang and Hancock (2004) that the outward deflecting sections are stiffer than the inward deflecting sections for thin materials. For thin materials (e.g. 1 mm), it can seen in Fig. 5 that for loads up to approximately 90 % of the failure load, which is approximately 1.3 P_{crd}, there is not much difference between the elastic and inelastic behaviour of the section. Hence this section is useful to demonstrate how distortional buckling interacts with local buckling. This will be further discussed when the stress distribution across the section is analysed.

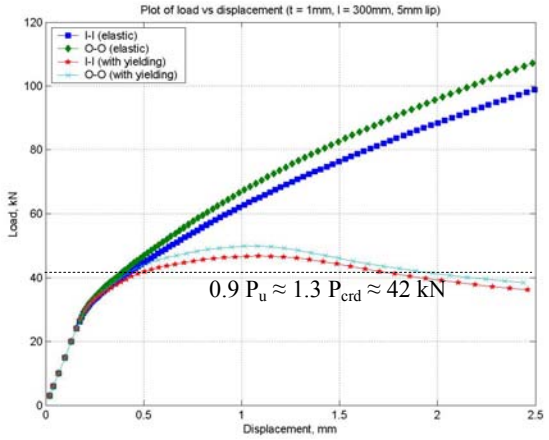

Figure 5 Load deflection curves for section with t = 1mm

Longitudinal stress distributions

The main objective of this paper is to investigate the post-distortional stress distribution and the effects of post-local buckling on post-distortional buckling behaviour, therefore sections with thicknesses 6 mm and 1 mm are chosen. The 6 mm section demonstrates a section undergoing post-distortional stress redistribution while at the other extreme, the section with 1 mm thickness demonstrates the effects of distortional buckling on the post-local buckling stresses.

Section with 6 mm thickness

The longitudinal stress distributions for the section with inward (I-I) and outward (O-O) deflections when the material is assumed to remain elastic is shown in Figs. 6a and b respectively. The analysis of the section with this thickness was chosen because it had an elastic distortional buckling stress (F_{crd} = 2132 MPa) much less than the elastic local buckling stress (F_{crl} = 5347 MPa). The ratio of F_{crl} to F_{crd} is approximately 2.51. For both cases, the sections deformed in the post-distortional mode since the stresses were well below those where local buckling effects might have affected it.

When the stresses are redistributed across the web in the post-distortional buckling region, the stresses decrease in the middle as it sheds the stresses to the flange-web junctions. However for the inward and outward deflections, the increased stresses at the junctions are different at similar load levels. When P/P_{crd} is approximately 1.35, the stress at the flange-web junction is approximately 3890 MPa for the inward deflection mode, while the stress at the flange-web junction for the outward deflection mode is approximately 4350 MPa. Thus it can be noted that in the post-distortional range, the flange-web junction of the outward mode carries more load than the inward mode at the same load level for a section with thickness 6 mm. This increased stress capacity for the section with outward deflection mode compared to the inward deflection mode indicates that the inward deflection mode is much softer as it sheds the load more rapidly as the deformations progress, as shown in Fig. 7. This confirms the results obtained by Yang and Hancock (2004) that the outward deflection modes are stiffer than the inward deflection modes.

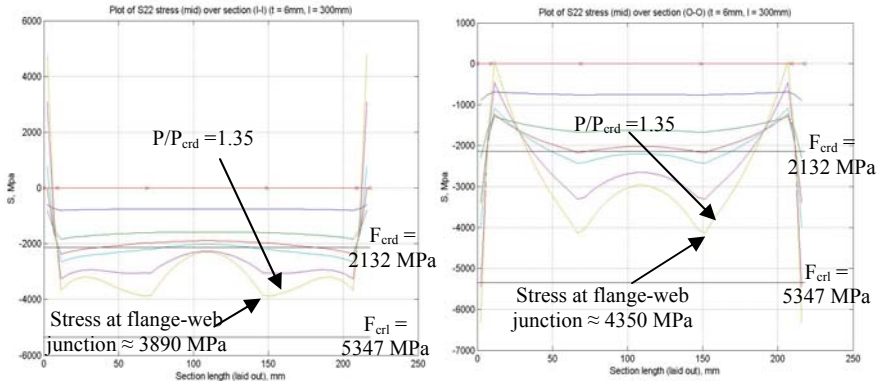

a) Inward deflection **b) Outward deflection**

Figure 6 Longitudinal stress distributions (I-I) and (O-O) around section t = 6 mm

When the distortional mode was "locked out" so as to observe the local buckling stress alone at the distortional length, the stress distribution for the post-local buckling range for the section is as shown in Fig. 8. It can be seen that as the load increases, there is significant stress redistribution in the middle of the web and flanges to the flange-web and flange-lip junctions as for normal post-local buckling behaviour. Figs. 6a and b also show that as the loads increase into the post-distortional buckling region, the stresses in the middle of the web and flanges are redistributed to the flange-web and flange-lip junctions. However, it is interesting to note that this post-distortional buckling stress redistribution has a unique characteristic which has some similarities to the post-local buckling stress distribution shown in Fig. 8, particularly for the inward deflection mode shown in Fig. 6a.

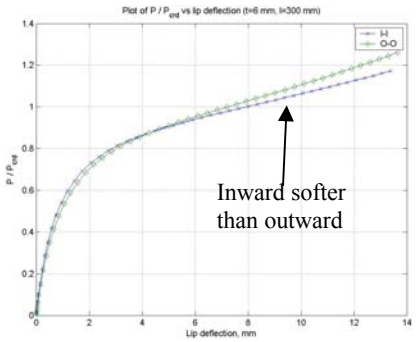

Figure 7 Plot of P/P_{crd} vs lip deflection for section t = 6mm

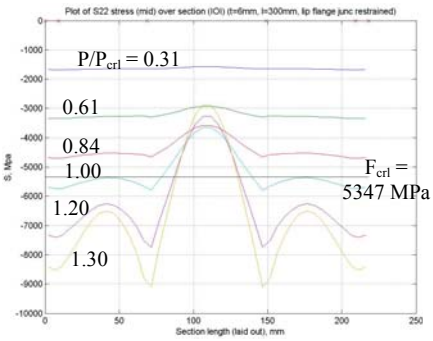

Figure 8 Longitudinal stress around section (forced local)

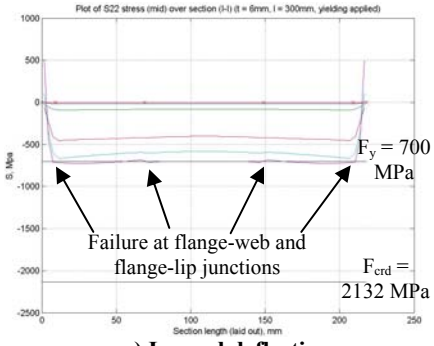

a) Inward deflection

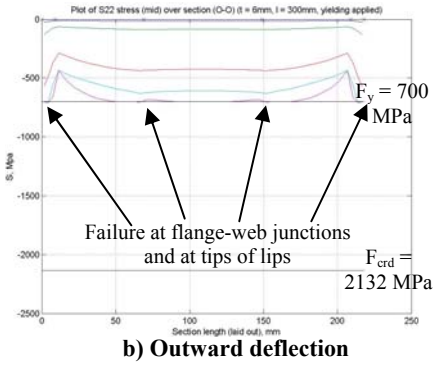

b) Outward deflection

Figure 9 Longitudinal stress distribution (I-I) and (O-O) around section t = 6mm (yielding included)

The longitudinal stress distributions for the section with inward and outward deflection cases now including yielding is shown in Figs. 9a and b respectively. For the section with inward deflection, the stress at the web and flanges are redistributed to the flange-web and flange-lip junctions relatively equally and hence yield approximately at the same time. The stress in the web and flanges for the section with the outward deflection are redistributed differently with most of the stress being shed to the lips and flange-web junctions. Due to the stress concentrating at the junction, the section fails at a slightly lower load when compared to the inward mode, with the lips yielding first but failure occurring in the junctions.

Section with 1 mm thickness

The longitudinal stress distributions for the section with inward (I-I) and outward (O-O) deflections when the material is assumed to remain elastic is shown in Figs. 10a and b respectively. The analysis of the section with this thickness was chosen because it had an elastic distortional buckling stress (F_{crd} = 154 MPa) is approximately equal to the elastic local buckling stress (F_{crl} = 163 MPa). The ratio of F_{crl} to F_{crd} is approximately 1.06. When P/P_{crd} is approximately 1.3, the stress at the flange-web junction is approximately 420 MPa for the inward deflection mode, while the stress at the flange-web junction for the outward deflection mode is approximately 400 MPa. It is interesting to note that at this thickness, the stress at the flange-web junction for the inward deflection is now higher than the outward deflection.

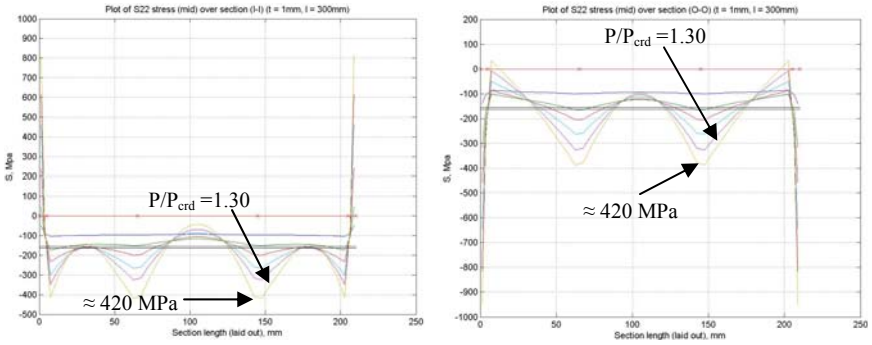

a) Inward deflection **b) Outward deflection**

Figure 10 Longitudinal stress distributions (I-I) and (O-O) for section t = 1mm

The lip displacements of the deflection modes are shown in Fig. 11 and although, as mentioned earlier, the flange-web junction of the outward deflection mode carries slightly more load than the junction of the inward

deflection mode, it can be seen that the inward deflection mode is softer than the outward deflection mode. This confirms the results obtained by Yang and Hancock (2004) that the outward deflection modes are stiffer than the inward deflection modes. With this increased stiffness, the outward mode fails at a higher load compared to the inward mode, as shown in the results in Fig. 2.

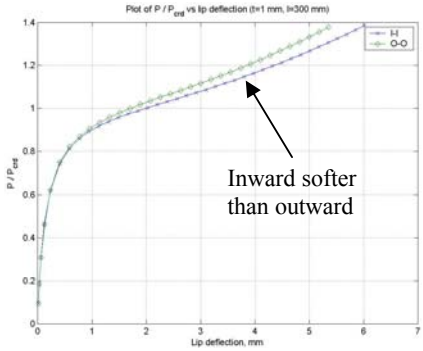

Figure 11 Plot of P/P_{crd} vs lip deflection for section t = 1mm

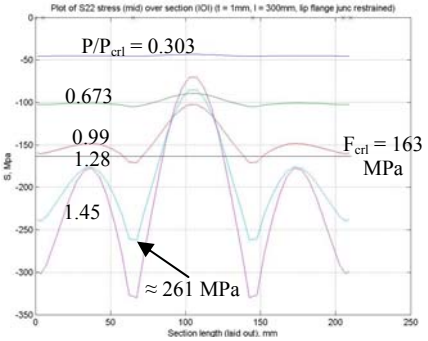

Figure 12 Longitudinal stress around section (forced local)

When the distortional mode was "locked out" so as to observe the local buckling stress at the distortional length, the stress distribution for the post-local buckling range for the section is as shown in Fig. 12. When the load applied was approximately 1.28 P_{crl}, which is equivalent to approximately 1.36 P_{crd}, the stress at the flange-web junction is approximately 261 MPa as shown in Fig. 12. This post-local buckling stress of 261 MPa can be compared to the stress at the flange-web junction at 1.3 P_{crd} (420 MPa) for the inward deflection mode (Fig. 10a). This comparison shows that the effect of distortional buckling on post-local buckling stress is to push the stress higher at the flange-web junctions. This shows the interaction of local and distortional buckling in the postbuckling range, which can be described by comparing Figs. 10a and 12. In Fig. 12, as the load increases into the post-local buckling range, 0.99 P_{crl} to 1.45 P_{crl}, the stresses in the centre of the web decreases to approximately 70 MPa, while the stresses in the flanges increase to approximately 175 MPa. This increased stress at the middle of the flange causes less stress to be redistributed to the junctions. In Fig. 10a, as the load increases into the post-distortional buckling range, 1.0 P_{crd} to 1.3 P_{crd}, the stress in the web decreases in a similar fashion to the post-local buckling behaviour. However the stresses in the flanges decrease very slightly and are redistributed into the junctions, causing the flange-web junctions to be more highly stressed.

The longitudinal stress distributions for the section with inward and outward deflection cases with yielding are shown in Figs. 13a and b respectively. The purpose of analysing both with and without yielding at this thickness was to observe whether the lip failure significantly influenced the behaviour. It can be observed for the inward deflection mode that up to 90 % of the failure load, which is approximately 1.3 P_{crd} as seen in Fig. 5, there is not much difference between the elastic and inelastic behaviour around the section except maybe the stresses in the centre of the flanges as shown in Figs. 10a and 13a. The maximum load still does not occur until the flange-web junction yielding occurs. Hence, although the lip yielding does cause some readjustment of the stresses, it is still the flange-web junction failure which governs the failure of the section and failure for the inward deflection mode occurs at a load of 1.445 P_{crl}. By comparison with the inward deflection mode, the outward mode fails at the yielding of the lips even though this is a higher load (1.54 P_{crd}) due to the different stress distributions as seen in Fig. 13b.

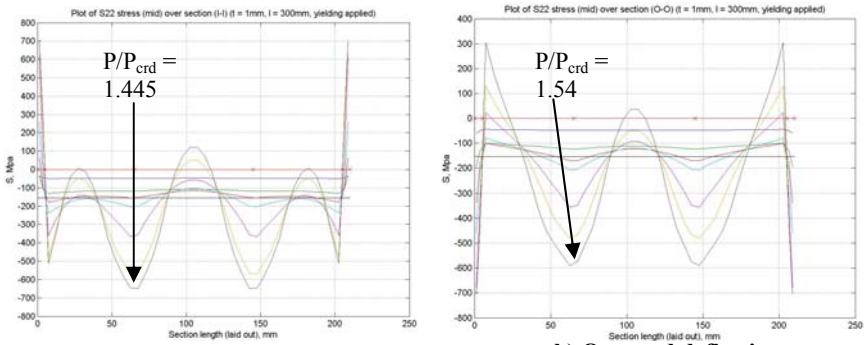

a) Inward deflection **b) Outward deflection**

Figure 13 Longitudinal stress distributions (I-I) and (O-O) around section t = 1mm (yielding included)

Effect of lip yielding on failure loads

It was previously discussed that a section with thickness 1 mm, lip yielding may occur but not cause failure of the section and that it is the flange-web junction that is normally the critical factor. A new section with increased yield stress applied to the lips was designed to further understand the effect of lip yielding on failure load.

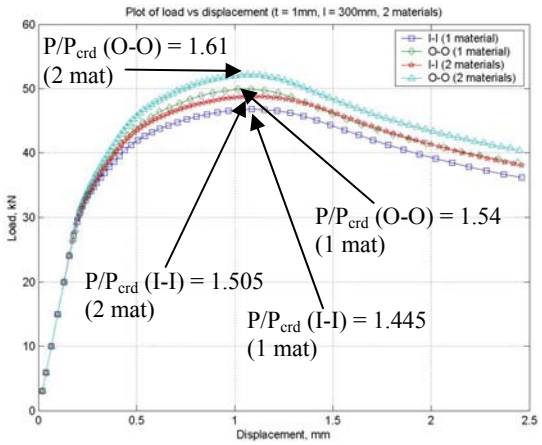

Figure 14 Load deflection curve for section t =1mm (2 materials)

Fig. 14 compares the load displacement plots for the inward and outward deflection modes for the sections with both one and two materials. With two materials, the inward deflection mode failed at approximately 1.505 P_{crd} and this presents a 4.15% increase in failure load of 1.445 P_{crd}, as shown in Fig. 13a for the section with one material. This increase is considered to be not significant. For the outward deflection mode, it can be seen from Fig. 14 that the failure load is 1.61 P_{crd} and this presents a 4.48 % increase from the failure load of 1.54 P_{crd} as shown in Fig. 13b for the section with one material. This increase is considered to be not significant. Therefore it can be concluded that lip yielding does not play a large part in the section failure while failure occurs very soon after yielding at the flange-web junction. This is confirmed by Yang (2004) with the 800 mm column failing in the outward deflection mode where local failure occurred in the lips at about 18 kN but the section continued to carry load to approximately 22 kN with very little apparent effect.

Test results in relation to strength design curves with 0.5 and 0.6 coefficients

The test results in relation to the Kwon and Hancock and Winter strength curves have been discussed by Yap and Hancock (2006). The paper noted that when the ratio of elastic local to distortional buckling stress is approximately 1.0, i.e. 1 mm (5mm lip) thick section, interaction of local and distortional buckling would most likely occur and cause the test results to be lower than the Kwon and Hancock strength curve as seen in Fig. 3. When a section has interaction of

buckling modes, the effect of this interaction causes the section to have a strength reduction of approximately 9.3 % to 10 %. The current design strength equations are unable to account for the interaction of buckling modes.

Conclusions

This paper has described the finite element analysis and results of the postbuckling in the local and distortional modes of thin-walled section with edge stiffeners of varying thicknesses. A sensitivity analysis for the magnitude of geometric imperfections in the distortional mode of the columns was carried out and the results were compared to known strength curves to validate the methodology against tests.

Longitudinal stress distributions have been discussed for sections failing purely in the distortional mode and with interaction of buckling modes. The effect of the post-distortional buckling mode on the post-local buckling stress distributions was to push the stress higher in the flange-web junctions. Failure tends to occur very soon after yielding of the flange-web junctions and lip yielding does not play a large part in the failure as had been predicted in earlier papers. The Winter strength curve is validated by the local buckling analyses, while the distortional buckling analyses showed that the Kwon and Hancock strength curve validates the FEA results with pure distortional failure modes. The interaction of local and distortional buckling modes indicated that there would be a reduction in section strength when the local and distortional buckling stresses are approximately equal.

The conclusions of this paper afford a much better understanding of failure in the post-distortional mode. In particular, the reasons why channel sections have a post-distortional strength which is not as significant as post-local strength have been explained. Further research is required to quantify the reductions due to the interaction of local and distortional buckling modes now that the mechanism is understood.

Appendix – References

American Iron and Steel Institute (AISI), (2004) Supplement 2004 to the North American Specification for the design of cold-formed steel structural members, 2001 edition, Washington, D.C.

Camotim, D., Silvestre, N., (2004) GBT-based analysis of the distortional postbuckling behaviour of cold-formed steel Z-section columns and beams, Proceedings of Fourth

International Conference on Thin-Walled Structures (Loughborough, 22-24/6), 2004, pp 243-250.

Hancock, G. J., (1985) Distortional buckling of steel storage rack columns, J Struct. Eng., v111, n 12, Dec 1985, pp 2770-83.

Hancock G. J., (2003) Cold-formed steel structures, Journal of Constructional Steel Research, v59(4), April 2003, pp 473-487.

Hancock G. J., Murray T.M. and Ellifritt D.S., (2001) Cold-formed steel structures to the AISI Specification. , Marcel Dekker, New York (2001).

Kwon Y. B. and Hancock G. J., (1992) Tests of cold-formed channels with local and distortional buckling. J Struct. Eng., v117(7), pp 1786-1803.

Lau, S. C. W. and Hancock, G. J. (1990) Inelastic buckling of channel columns in the distortional mode, Thin-Walled Structures, Vol. 10, Issue 1, 1990, pp 59-84.

Schafer B.W., Pekoz T., (1998) Computational modelling of cold-formed steel: characterizing geometric imperfections and residual stresses. Journal of Constructional Research, 1998, v 47, pp 193-210.

Schafer, B.W., (2002) Local, distortional, and Euler buckling of thin-walled columns, J Struct. Eng., v 128, n 3, March 2002, pp 289-299.

Silvestre, N. and Camotim, D., (2004) Local-plate and distortional post-buckling behaviour of cold-formed steel lipped channel columns with intermediate stiffeners, Proceedings of Seventeen International Speciality Conference on Cold-Formed Steel Structures (Orlando, 4-5/11), 2004, pp 1-18.

Sridharan, S., (1982) Semi-analytical method for the post-local-torsional buckling analysis of prismatic plate structures, Int. J. Numer. Methods Eng., v 18, n 11, Nov 1982, pp 1685-1697.

Standards Australia / Standards New Zealand (2005), Cold-formed steel structures-AS/NZS 4600:2005, Sydney, NSW, Australia.

Timoshenko, S.P., (1945) Theory of bending, torsion and buckling of thin-walled members of open cross section, Journal of the Franklin Institute, Vol 239, Issue 5, May 1945, pp 343-361.

Trahair, N. S., (1993) Flexural-torsional buckling of structures, First edition, E & F N Spon, 1993.

Vlasov, V. Z., (1961) Thin-walled elastic beams, Moscow (English translation Israel Program for Scientific Translation, Jerusalem), 1961.

Von Karman, T., Sechler, E.E. and Donnell, L.H., (1932) The strength of thin plates in compression, Transactions ASME, Vol. 54, MP 54-5, 1932.

Winter, G., (1968) Thin-walled structures-Theoretical solutions and test results. Preliminary Publications of the Eighth Congress, IABSE, 1968, pp 101-112.

Yang, D. and Hancock, G.J., (2004) Compression Tests of Cold-Reduced High Strength Steel Channel Columns Failing in the Interaction Between Local and Distortional Modes. Journal of Structural Engineering, Vol. 130, No 12, pp 1954-1963.

Yang, D., (2004) Compression Stability of High Strength Steel Sections with Low Strain-Harding, Ph.D. Thesis, School of Civil Engineering, University of Sydney.

Yap, D.C.Y., Hancock, G.J., (2006) Interaction buckling and postbuckling in the distortional mode of thin-walled sections, Research Report No. R870, School of Civil Engineering, University of Sydney, Sydney, NSW, Australia, April, 2006.